

**PERVAPORATION MEMBRANE CONTAINING  
ELECTROSPUN POLY(VINYL ALCOHOL)  
COMPOSITE NANOFIBRE LAYER FOR  
DEHYDRATION OF 1,4-DIOXANE**

**YEANG QIAN WEN**

**UNIVERSITI SAINS MALAYSIA**

**2018**

**PERVAPORATION MEMBRANE CONTAINING ELECTROSPUN  
POLY(VINYL ALCOHOL) COMPOSITE NANOFIBRE LAYER FOR  
DEHYDRATION OF 1,4-DIOXANE**

**by**

**YEANG QIAN WEN**

**Thesis submitted in fulfillment of the  
requirements for the degree of  
Doctor of Philosophy**

**December 2018**

## ACKNOWLEDGEMENT

First and foremost, I would like to convey my heart-felt gratitude to my dedicated supervisor, Associate Professor Dr. Tan Soon Huat and co-supervisor, Associate Professor Ir. Dr. Abu Bakar Sulong for their excellent supervision and guidance throughout my research. Despite their busy schedule, they were willing to provide invaluable assistance in offering constructive comments and suggestions based on their immense knowledge in my field of study. Without their support, this research project would not have come this far.

Next, I would like to express my sincere gratitude to my fellow friends and colleagues, Kin Hang, Swee Pin, Yit Thai, Siew Hoong, Kian Fei, Huey Ping, who had given me their support during the ups and downs of my PhD journey. Their physical, spiritual and mental support gave me motivation to strive for the completion of this research.

Besides that, I would like to express my appreciation to our respected Dean, Professor Dr. Azlina Bt. Harun @ Kamaruddin, Deputy Dean, Associate Professor Ir. Dr. Zainal Ahmad and Professor Dr. Ahmad Zuhairi Abdullah for the guidance throughout my research in USM. Also, I would like to express my gratitude to all the administrative staffs and laboratory assistant engineers of School of Chemical Engineering, USM for giving me full support throughout my research.

Also, my deepest and heart-felt gratitude towards my beloved parents and siblings for their endless love and encouragement throughout my studies.

Not forgotten, my grateful acknowledgement to the financial supports from MyPhd fellowship from the Ministry of Higher Education of Malaysia and the Fundamental Research Grant Scheme (FRGS) (A/C:6071295).

Finally, I would like to thank those who indirectly contributed to this research, including those that I might have missed out. Their contributions and kindness are greatly appreciated.

Thank you very much!

*Yeang Qian Wen, 2018*

## TABLE OF CONTENTS

	<b>Page</b>
<b>ACKNOWLEDGEMENT</b>	ii
<b>TABLE OF CONTENTS</b>	iv
<b>LIST OF TABLES</b>	ix
<b>LIST OF FIGURES</b>	xi
<b>LIST OF ABBREVIATIONS</b>	xv
<b>LIST OF SYMBOLS</b>	xvii
<b>ABSTRAK</b>	xix
<b>ABSTRACT</b>	xxi
<b>CHAPTER ONE: INTRODUCTION</b>	
1.1 Pervaporation	1
1.2 Current development of membrane for pervaporation	3
1.2.1 Polymeric membrane	6
1.2.2 Inorganic membrane	7
1.2.3 Mixed-matrix membranes (MMMs)	8
1.3 Electrospun nanofibres and their applications	10
1.4 Problem Statement	11
1.5 Objectives	14
1.6 Scope of the study	14
1.7 Organization of the thesis	16
<b>CHAPTER TWO: LITERATURE REVIEW</b>	
2.1 Fabrication of electrospun nanofibres via electrospinning process	18
2.1.1 Working principle	19
2.1.2 Effects of various parameters on electrospinning	21

2.1.2(a)	Solution parameters	22
2.1.2(a)(i)	Polymer concentration	22
2.1.2(a)(ii)	Molecular weight	22
2.1.2(a)(iii)	Viscosity	23
2.1.2(a)(iv)	Surface tension	25
2.1.2(b)	Processing parameters	25
2.1.2(b)(i)	Applied voltage	25
2.1.2(b)(ii)	Tip to collector distance	26
2.1.2(b)(iii)	Flow rate of solution	27
2.1.2(b)(iv)	Types of collectors	27
2.2	Electrospun nanofibres in membrane separation processes	28
2.2.1	Pressure-driven membrane processes	28
2.2.2	Osmotically driven membrane processes	32
2.2.3	Membrane distillation	34
2.2.4	Pervaporation	36
2.3	Metal organic frameworks (MOFs): Cu-BTC	37
2.4	Carbon nanotubes (CNTs)	39
2.5	Application of nanomaterials incorporated MMMs in pervaporation process	41
2.5.1	MOFs	41
2.5.2	CNTs	48
2.6	Pervaporation dehydration of 1,4-dioxane/water mixture	55
2.7	Fundamental on the estimation of transport coefficient using Rautenbach model	58
2.8	Summary	61

### **CHAPTER THREE: MATERIALS AND METHODOLOGY**

3.1	Raw materials and chemicals	63
3.1.1	Raw materials	63
3.1.2	Chemicals	63
3.2	Overall research methodology	64
3.3	Synthesis of $\text{Cu}_3(1,3,5\text{-benzenetricarboxylate})_2$ , Cu-BTC	66
3.4	Fabrication of asymmetric membranes	67

3.4.1	Fabrication of asymmetric membrane with pre-selective layer of electrospun PVA nanofibres ( $M_0$ )	67
3.4.2	Fabrication of asymmetric membrane with pre-selective layer of electrospun Cu-BTC/PVA nanofibres ( $M_{CuBTC}$ )	68
3.4.3	Fabrication of asymmetric membrane with pre-selective layer of electrospun COOH-MWCNT/PVA nanofibres ( $M_{COOH-MWCNT}$ )	69
3.5	Characterization	70
3.5.1	Brunauer-Emmett-Teller (BET)	70
3.5.2	Scanning electron microscopy (SEM)	70
3.5.3	Transmission electron microscopy (TEM)	70
3.5.4	Fourier transform infrared (FTIR) analysis	71
3.5.5	Capillary flow porometer	71
3.5.6	Contact angle measurement	71
3.6	Liquid sorption study	72
3.7	Pervaporation	73
3.7.1	Pervaporation operation	73
3.7.2	Pervaporation process study	74
3.7.3	Evaluation of pervaporation performance	76
3.7.4	Estimation of the transport coefficient in pervaporation using the Rautenbach model	77

## **CHAPTER FOUR: RESULTS AND DISCUSSION**

4.1	Characterization of Cu-BTC and $M_{CuBTC}$	82
4.1.1.	Brunauer-Emmett-Teller (BET) surface area analysis and total pore volume of Cu-BTC	82
4.1.2	Scanning electron microscopy (SEM)	82
4.1.3	Fourier transform infrared (FTIR) analysis	85
4.1.4	Pore size distribution of the electrospun pre-selective nanofibre layer	86
4.1.5	Contact angle measurement	87
4.2	Liquid sorption study	87
4.3	Pervaporation performance of $M_{CuBTC}$ in the dehydration of 1,4-dioxane/water mixtures	91
4.3.1	Effect of the electrospun Cu-BTC/PVA layer of the asymmetric membranes on pervaporation	91

4.3.2	Effect of feed water concentration	96
4.3.3	Effect of feed temperature	99
4.4	Characterization of COOH-MWCNTs and $M_{\text{COOH-MWCNT}}$	104
4.4.1	Brunauer-Emmett-Teller (BET) surface area analysis and total pore volume of COOH-MWCNT	104
4.4.2	Transmission electron microscopy (TEM) images of COOH-MWCNT and electrospun COOH-MWCNT/PVA nanofibre	105
4.4.3	Scanning electron microscopy (SEM)	106
4.4.4	Fourier transform infrared (FTIR) analysis	107
4.4.5	Pore size distribution of the electrospun pre-selective nanofibre layer	109
4.4.6	Contact angle measurement	109
4.5	Liquid sorption study	110
4.6	Pervaporation performance of $M_{\text{COOH-MWCNT}}$ in dehydration of 1,4-dioxane/water mixtures	113
4.6.1	Effect of the electrospun COOH-MWCNT/PVA layer of the asymmetric membranes on pervaporation	113
4.6.2	Effect of feed water concentration	117
4.6.3	Effect of feed temperature	121
4.7	Comparison of the pervaporation performances of the asymmetric membranes $M_{\text{CuBTC}}$ and $M_{\text{COOH-MWCNT}}$	126
4.8	Comparison of the present pervaporation performance with literature reported data	128
4.9	Estimation of the transport coefficient in pervaporation using the Rautenbach model	130
4.9.1	Estimation of the transport coefficient in pervaporation through the $M_{\text{CuBTC}(1.0)}$ asymmetric membrane	130
4.9.2	Estimation of the transport coefficient in pervaporation through the $M_{\text{COOH-MWCNT}(0.5)}$ asymmetric membrane	139
4.9.3	Comparison of the Rautenbach model-predicted parameters of the $M_{\text{CuBTC}(1.0)}$ and $M_{\text{COOH-MWCNT}(0.5)}$ asymmetric membranes	147

## **CHAPTER FIVE: CONCLUSIONS AND RECOMMENDATIONS**

5.1	Conclusions	151
5.2	Recommendations	153

## **REFERENCES**

154

## **APPENDICES**

- Appendix A Calculation of sorption properties
- Appendix B Calculation of pervaporation performances
- Appendix C Calculation of activity coefficients
- Appendix D Estimation of transport coefficients

## **LIST OF PUBLICATIONS**

## LIST OF TABLES

		<b>Page</b>
Table 2.1	Performance of various membranes in pervaporation dehydration of 1,4-dioxane.	59
Table 3.1	List of chemicals used in this research work	64
Table 3.2	Experimental studies on the effect of feed concentration of water for dehydration of 1,4-dioxane.	75
Table 3.3	Experimental studies on the effect of feed temperature for dehydration of 1,4-dioxane.	75
Table 4.1	Pore size distribution of the electrospun pre-selective nanofibre layer of $M_0$ , $M_{CuBTC(0.5)}$ and $M_{CuBTC(1.0)}$ .	86
Table 4.2	Comparison of contact angle measurements of dense PVA, $M_0$ , $M_{CuBTC(0.5)}$ and $M_{CuBTC(1.0)}$ .	87
Table 4.3	Comparison of the sorption selectivities of dense PVA, $M_0$ , $M_{CuBTC(0.5)}$ and $M_{CuBTC(1.0)}$ in 95 wt.% 1,4-dioxane/5 wt. % water.	90
Table 4.4	Performance of $M_{CuBTC(1.0)}$ for the pervaporation dehydration of 95 wt.% 1,4-dioxane/5 wt.% water mixture at 30°C and 5 mmHg.	96
Table 4.5	Pore size distribution of the electrospun pre-selective nanofibre layer of $M_0$ , $M_{COOH-MWCNT(0.5)}$ and $M_{COOH-MWCNT(1.0)}$ .	109
Table 4.6	Measured contact angles of dense PVA, $M_0$ , $M_{COOH-MWCNT(0.5)}$ and $M_{COOH-MWCNT(1.0)}$ .	110
Table 4.7	Comparison of the sorption selectivities of dense PVA, $M_0$ , $M_{COOH-MWCNT(0.5)}$ and $M_{COOH-MWCNT(1.0)}$ in 95 wt.% 1,4-dioxane/5 wt. % water	113
Table 4.8	Performance of $M_{COOH-MWCNT(0.5)}$ for the pervaporation dehydration of 95 wt.% 1,4-dioxane/5 wt.% water mixture at 30°C and 5 mmHg.	118
Table 4.9	Comparison with available literature on the pervaporation dehydration of 1,4-dioxane/water mixture.	129

Table 4.10	Activation energies, relative transport coefficients and enthalpies of sorption of water and 1,4-dioxane of the $M_{CuBTC(1.0)}$ asymmetric membrane.	131
Table 4.11	Experimental and predicted transport coefficient, $\bar{D}$ of water and 1,4-dioxane in the $M_{CuBTC(1.0)}$ asymmetric membrane at different feed temperature.	134
Table 4.12	$R^2$ values for the permeation fluxes of water and 1,4-dioxane and separation factor of the $M_{CuBTC(1.0)}$ predicted with Rautenbach equation.	138
Table 4.13	Activation energies, relative transport coefficients and enthalpies of sorption of water and 1,4-dioxane of the $M_{COOH-MWCNT(0.5)}$ asymmetric membrane.	140
Table 4.14	Experimental and predicted transport coefficient, $\bar{D}$ of water and 1,4-dioxane in the $M_{COOH-MWCNT(0.5)}$ asymmetric membrane at different feed temperature.	143
Table 4.15	$R^2$ values for the permeation fluxes of water and 1,4-dioxane and separation factor of the $M_{COOH-MWCNT(0.5)}$ predicted with Rautenbach equation.	147
Table 4.16	Comparison of the activation energies, relative transport coefficients and enthalpies of sorption of water and 1,4-dioxane of the $M_{CuBTC(1.0)}$ and $M_{COOH-MWCNT(0.5)}$ asymmetric membranes.	147
Table 4.17	Comparison of the predicted transport coefficient, $\bar{D}$ of water and 1,4-dioxane in the $M_{CuBTC(1.0)}$ and $M_{COOH-MWCNT(0.5)}$ asymmetric membranes at different feed temperature.	149

## LIST OF FIGURES

		<b>Page</b>
Figure 1.1	Schematic diagram of the pervaporation process (Feng and Huang, 1997).	2
Figure 1.2	Graphical representation of the solution-diffusion mechanism (Ong et al., 2016).	4
Figure 1.3	Schematic diagram of a MMM.	9
Figure 1.4	Schematic diagram of the proposed asymmetric membrane.	13
Figure 2.1	A basic electrospinning set up (Bhardwaj and Kundu, 2010).	20
Figure 2.2	Schematic illustration of the Taylor cone formation: (A) Surface charges are induced in the polymer solution due to the electric field. (B) Elongation of the pendant drop. (C) Deformation of the pendant drop to the form the Taylor cone due to the charge-charge repulsion. A fine jet initiates from the cone (Baji et al., 2010).	21
Figure 2.3	Variation in morphology of electrospun nanofibres of poly(ethylene oxide) PEO with increasing viscosity: (a–d) schematic and (e–h) SEM micrographs (Haider et al., 2015).	24
Figure 2.4	Flexible assembly process of MOFs from metal nodes and organic linkers (Burtch et al., 2014).	38
Figure 2.5	Dimeric cupric tetracarboxylate unit and unit cell crystal structure of Cu-BTC (Cu: light pink; C: grey; H: white and O: red) (Yang et al., 2013).	39
Figure. 2.6	Schematic structures of (a) single-walled CNT (SWCNT) and (b) multi-walled CNTs (MWCNT) (Dubey et al., 2017). Transmission electron microscopy (TEM) images of (c) SWCNT (Vadahanambi et al., 2013) and (d) MWCNT (Yee et al., 2014).	40
Figure 3.1	Schematic diagram of the overall research methodology.	65
Figure 3.2	Schematic diagram of the electrospinning setup.	68
Figure 3.3	Schematic diagram of the pervaporation test rig.	74
Figure 4.1	SEM images of Cu-BTC crystals at (a) 3000× and (b) 10000× magnification.	82

Figure 4.2	SEM images of PVA nanofibres electrospun using PVA solutions with concentration of (a) 6, (b) 7 and (c) 8 wt.%.	83
Figure 4.3	Surface and cross-sectional SEM images of (a and b) the $M_{CuBTC}$ membrane and (c and d) the $M_0$ membrane.	84
Figure 4.4	FTIR spectra of Cu-BTC, PVA membrane and $M_{CuBTC}$ membrane.	86
Figure 4.5	Degree of swelling of dense PVA, $M_0$ , $M_{CuBTC(0.5)}$ and $M_{CuBTC(1.0)}$ in various solutions.	89
Figure 4.6	Composition of liquid sorbed by $M_{CuBTC(0.5)}$ in various feed solutions.	89
Figure 4.7	Composition of liquid sorbed by $M_{CuBTC(1.0)}$ in various feed solutions.	90
Figure 4.8	Permeation fluxes and separation factors of dense PVA, $M_0$ , $M_{CuBTC(0.5)}$ and $M_{CuBTC(1.0)}$ when used for dehydration pervaporation of 95 wt.% 1,4-dioxane solution at 30 °C and downstream pressure of 5 mmHg.	92
Figure 4.9	Schematic diagrams of (a) dense PVA, (b) $M_0$ , and (c) $M_{CuBTC}$ membranes.	93
Figure 4.10	Effects of the concentration of water in the feed on (a) the permeation flux, (b) the permeate concentration and separation factor and (c) the permeance and selectivity of the $M_{CuBTC(1.0)}$ membrane at 30 °C and downstream pressure of 5 mmHg.	97
Figure 4.11	Effects of the feed temperature on (a) the permeation flux, (b) the permeate concentration and separation factor and (c) the permeance and selectivity of the $M_{CuBTC(1.0)}$ membrane with a feed of 95 wt.% 1,4-dioxane and a downstream pressure of 5 mmHg.	100
Figure 4.12	Arrhenius plots of (a) the permeation flux and (b) the permeance of $M_{CuBTC(1.0)}$ with a feed of 95 wt.% 1,4-dioxane and a downstream pressure of 5 mmHg.	103
Figure 4.13	TEM images of (a) COOH-MWCNT and (b) electrospun COOH-MWCNT/PVA nanofibre.	105
Figure 4.14	Surface and cross-sectional SEM images of (a and b) the $M_{COOH-MWCNT}$ membrane and (c and d) the $M_0$ membrane.	107

Figure 4.15	FTIR spectra of COOH-MWCNT, PVA membrane, and M <sub>COOH-MWCNT</sub> membrane.	108
Figure 4.16	Degree of swelling of dense PVA, M <sub>0</sub> , M <sub>COOH-MWCNT(0.5)</sub> and M <sub>COOH-MWCNT(1.0)</sub> in various solutions.	111
Figure 4.17	Composition of liquid sorbed by M <sub>COOH-MWCNT(0.5)</sub> in various feed solutions.	112
Figure 4.18	Composition of liquid sorbed by M <sub>COOH-MWCNT(1.0)</sub> in various feed solutions.	112
Figure 4.19	Permeation fluxes and separation factors of dense PVA, M <sub>0</sub> , M <sub>COOH-MWCNT(0.5)</sub> and M <sub>COOH-MWCNT(1.0)</sub> when used for dehydration pervaporation of 95 wt.% 1,4-dioxane solution at 30 °C and downstream pressure of 5 mmHg.	114
Figure 4.20	Schematic diagram showing the interaction of water molecules with electrospun M <sub>COOH-MWCNT</sub> membrane.	115
Figure 4.21	Effects of the concentration of water in the feed on (a) the permeation flux, (b) the permeate concentration and separation factor and (c) the permeance and selectivity of the M <sub>COOH-MWCNT(0.5)</sub> membrane at 30 °C and downstream pressure of 5 mmHg.	119
Figure 4.22	Effects of the feed temperature on (a) the permeation flux, (b) the permeate concentration and separation factor and (c) the permeance and selectivity of the M <sub>COOH-MWCNT(0.5)</sub> membrane with a feed of 95 wt.% 1,4-dioxane and a downstream pressure of 5 mmHg.	122
Figure 4.23	Arrhenius plots of (a) the permeation flux and (b) the permeance of M <sub>COOH-MWCNT(0.5)</sub> with a feed of 95 wt.% 1,4-dioxane and a downstream pressure of 5 mmHg.	125
Figure 4.24	Permeation fluxes and separation factors of M <sub>CuBTC(0.5)</sub> , M <sub>CuBTC(0.5)</sub> , M <sub>COOH-MWCNT(0.5)</sub> and M <sub>COOH-MWCNT(1.0)</sub> when used for dehydration pervaporation of 95 wt.% 1,4-dioxane solution at 30 °C and downstream pressure of 5 mmHg.	126
Figure 4.25	Arrhenius plot of the transport coefficient of water and 1,4-dioxane for M <sub>CuBTC(1.0)</sub> .	131
Figure 4.26	Parity plot of the predicted and experimental value of the transport coefficient, <i>D</i> of (a) water and (b) 1,4-dioxane at different feed temperature for M <sub>CuBTC(1.0)</sub> .	135
Figure 4.27	Plot of the (a) partial permeation flux of water and 1,4-dioxane and (b) separation factor over feed temperature for M <sub>CuBTC(1.0)</sub> .	137

Figure 4.28	Arrhenius plot of the transport coefficient of water and 1,4-dioxane for $M_{\text{COOH-MWCNT}(0.5)}$ .	140
Figure 4.29	Parity plot of the predicted and experimental value of the transport coefficient, $\bar{D}$ of (a) water and (b) 1,4-dioxane at different feed temperature for $M_{\text{COOH-MWCNT}(0.5)}$ .	143
Figure 4.30	Plot of the (a) partial permeation flux of water and 1,4-dioxane and (b) separation factor over feed temperature for $M_{\text{COOH-MWCNT}(0.5)}$ .	146

## LIST OF ABBREVIATIONS

[Bmim][BF <sub>4</sub> ]	1-butyl-3-methylimidazolium tetrafluoroborate
3D	3-dimensional
ABE	Acetone-butanol-ethanol
Al <sub>2</sub> O <sub>3</sub>	Aluminum oxide
Al-MCM-41	Alumina-containing mobile composition matter-41
BDC	Benzene dicarboxylate
BET	Brunauer-Emmett-Teller
BP	Buckypaper
BSA	Bovine serum albumin
BTC	Benzene-1,3,5 tricarboxylic acid or trimesic acid
CNT	Carbon nanotube
Co(HCOO) <sub>2</sub>	Co(II)-formate
COOH-MWCNT	Carboxyl multi-walled carbon nanotube
CS	Chitosan
Cu-BTC	Cu <sub>3</sub> (1,3,5-benzenetricarboxylate) <sub>2</sub>
CVD	Chemical vapour deposition
DMF	N,N-dimethylformamide anhydrous
Fe <sub>3</sub> O <sub>4</sub>	Magnetite
FTIR	Fourier transform infrared
GPU	Gas permeation units
IPA	Isopropanol
M <sub>0</sub>	Asymmetric membranes with electrospun PVA nanofibres as pre-selective layer
M <sub>COOH-MWCNT</sub>	Asymmetric membranes with electrospun COOH-MWCNT/PVA nanofibres as pre-selective layer
M <sub>CuBTC</sub>	Asymmetric membranes with electrospun Cu-BTC/PVA nanofibres as pre-selective layer
MMM	Mixed matrix membrane
MOF	Metal organic framework
MWCNT	Multi-walled carbon nanotube
PA	Polyamide

PAH	Poly(allylamine hydrochloride)
PAN	Poly(acrylonitrile)
PANI	Polyaniline
PBI	Polybenzimidazole
PDMS	Polydimethylsiloxane
PEBA	Poly(ether block amide)
PEC	Polyelectrolyte–polyelectrolyte complex
PEI	Polyethyleneimine
PES	Polyethersulfone
PET	Polyethylene terephthalate
PHB	Poly(3-hydroxybutyrate)
PI	Polyimide
PS	Polystyrene
PSF	Polysulfone
PSI	Pervaporation separation index
PSSA	Poly(styrene sulfonic acid)
PVA	Polyvinyl alcohol
PVDF	Polyvinylidene fluoride
SEM	Scanning electron microscope
SILM	Supported ionic liquid membrane
SPES	Sulfonated polyethersulfone
SPES-C	Sulfonated polyarylethersulfone with cardo
SWCNT	Single-walled carbon nanotube
TED	Triethylenediamine
TEM	Transmission electron microscopy
TiO <sub>2</sub>	Titanium dioxide
ZIF	Zeolitic imidazolate framework
β-CD	β-cyclodextrin

## LIST OF SYMBOLS

$\bar{\gamma}_i$	Average activity coefficient of component $i$ at the feed side and permeate side
$\bar{D}_i^*$	Relative transport coefficient of component $i$
$\Delta H_{Si}$	Enthalpy of sorption of component $i$
$A$	Effective membrane area
$A_{ij}$	Wilson parameter
$A_{ji}$	Wilson parameter
$\bar{D}_i$	Transport coefficient of component $i$
$E_{Di}$	Activation energy for diffusion of component $i$
$E_{Ji}$	Activation energy for the permeation of component $i$ which takes into account the impact of the driving force
$E_{Pi}$	Permeation activation energy, which characterises the dependence of the membrane permeance on the temperature
$J$	Permeation flux
$J_{i0}$	Pre-exponential factor of the permeation flux
$M_d$	Weight of the dry membrane
$M_s$	Weight of the swollen membrane
$MW_i$	Molar mass of component $i$ ,
$P$	Permeance
$p_{i1}$	Partial pressure of component $i$ at the liquid phase side of the membrane
$p_{i2}$	Partial pressure of component $i$ at the vapour phase side of membrane
$P_{i0}$	Pre-exponential factor of the permeance
$p_i^{sat}$	Saturated vapour pressure of component $i$ at the feed side
$p_p$	Downstream pressure at permeate side
$Q$	Amount of permeate collected
$Q_0$	Permeability of the porous layer of membrane
$R$	Universal gas constant
$T$	Absolute temperature
$T^*$	Reference temperature, equal to 293K

$X_i$	Weight fraction of component $i$ in the feed
$x_i$	Molar fraction of component $i$ at the feed side
$x_j$	Molar fraction of component $j$ at the feed side
$Y_i$	Weight fraction of component $i$ in permeate
$y_i$	Molar fraction of component $i$ at the permeate side
$Y_{im}$	Weight fraction of component $i$ in the membrane
$\alpha$	Separation factor
$\beta$	Membrane selectivity
$\beta_{diff}$	Diffusion selectivity
$\beta_{sorp}$	Sorption selectivity
$\gamma_{i1}$	Activity coefficient of component $i$ at the feed side
$\gamma_{i2}$	Activity coefficient of component $i$ at the permeate side
$\gamma_{j1}$	Activity coefficient of component $j$ at the feed side
$\delta$	Thickness of the asymmetric membrane
$\Delta t$	Time interval

**MEMBRAN PENYEJATTELAPAN DENGAN LAPISAN GENTIAN  
BENANG NANO KOMPOSIT POLI(VINIL ALKOHOL) HASILAN  
PEJAMAN ELEKTRIK UNTUK PENYAHHIDRATAN 1,4-DIOXAN**

**ABSTRAK**

Dalam kajian ini, membran asimetri baru dengan lapisan pra-memilih hasilan pejaman elektrik yang terdiri daripada gentian benang nano poli (vinil alkohol) (PVA) dan gentian benang nano komposit PVA yang bersepadu dengan dua jenis pengisi hidrofilik iaitu kuprum benzena-1,3,5-trikarboksilat (Cu-BTC) bersaiz mikron dan tiub-nano karbon dinding berlapis berfungsi kumpulan karboksil (COOH-MWCNT) bersaiz nano berjaya dihasilkan. Membran PVA dilapiskan dengan gentian benang nano PVA, gentian benang nano komposit Cu-BTC/PVA dan COOH-MWCNT/PVA untuk masing-masing membentuk membran asimetri  $M_0$ ,  $M_{CuBTC}$  dan  $M_{COOH-MWCNT}$ . Semua membran asimetri mempamerkan peningkatan prestasi dalam penyahhidratan 1,4-dioxan melalui proses penyejattelapan. Kejadian ini adalah kesan daripada lapisan pra-memilih berfungsi sebagai penapis hidrofilik yang memerangkap molekul air. Prestasi penyejattelapan membran meningkat dalam susunan berikut: membran PVA <  $M_0$  <  $M_{COOH-MWCNT}$  <  $M_{CuBTC}$ . Berbanding dengan membran PVA,  $M_0$  menunjukkan menunjukkan peningkatan hampir 50% dalam fluks penelapan air serentak dengan peningkatan dalam faktor pemisahan. Antara membran  $M_{CuBTC}$  dan  $M_{COOH-MWCNT}$ , membran  $M_{CuBTC}$  mempamerkan prestasi penyejattelapan yang lebih baik. Prestasi membran  $M_{CuBTC}$  meningkat dengan peningkatan kandungan Cu-BTC dari 0.5 hingga 1.0 wt.%. Di antara semua membran yang dikaji, membran  $M_{CuBTC}$  dengan 1.0 wt.% Cu-BTC ( $M_{CuBTC(1.0)}$ ) mempamerkan fluks telapan dan faktor

pemisahan tertinggi dengan jumlah fluks penelapan sebanyak  $87.69 \text{ g/m}^2\cdot\text{j}$ , faktor pemisahan sebanyak 1852.32, kebolehtelapan air yang bernilai 2176.20 GPU, dan kememilihan membran untuk air yang bernilai 1417.52. Fluks penelapan air yang ditunjukkan oleh membran  $\text{M}_{\text{CuBTC}(1.0)}$  adalah dua kali ganda daripada membran PVA, manakala faktor pemisahan meningkat dari 392.65 hingga 1852.32. Berbanding dengan  $\text{M}_0$ , membran  $\text{M}_{\text{CuBTC}(1.0)}$  menunjukkan peningkatan hampir 40% dalam fluks penelapan air bersama dengan peningkatan dalam faktor pemisahan. Walau bagaimanapun, di antara membran  $\text{M}_{\text{COOH-MWCNT}}$  dengan 0.5 dan 1.0 wt.% COOH-MWCNT, iaitu  $\text{M}_{\text{COOH-MWCNT}(0.5)}$  and  $\text{M}_{\text{COOH-MWCNT}(1.0)}$ , prestasi penyejattelapan yang lebih baik ditunjukkan oleh  $\text{M}_{\text{COOH-MWCNT}(0.5)}$  dengan jumlah fluks penelapan yang bernilai  $75.71 \text{ g/m}^2\cdot\text{j}$ , faktor pemisahan yang bernilai 605.35, kebolehtelapan air yang bernilai 1836.08 GPU dan kememilihan membran untuk air yang bernilai 462.30. Peningkatan sebanyak lebih kurang 80% dan 20% dalam fluks penelapan air ditunjukkan oleh  $\text{M}_{\text{COOH-MWCNT}(0.5)}$  berbanding dengan membran PVA dan  $\text{M}_0$  masing-masing. Walaupun faktor pemisahan  $\text{M}_{\text{COOH-MWCNT}(0.5)}$  meningkat daripada 392.65 kepada 605.35 berbanding dengan membran PVA, faktor pemisahan berkurang dari 682.11 kepada 605.35 berbanding dengan  $\text{M}_0$ . Paramater yang diramal dengan menggunakan model Rautenbach menunjukkan bahawa penyahhidratan 1,4-dioxan melalui proses penyejattelapan dikawal oleh proses penyerapan.

**PERVAPORATION MEMBRANE CONTAINING ELECTROSPUN  
POLY(VINYL ALCOHOL) COMPOSITE NANOFIBRE LAYER FOR  
DEHYDRATION OF 1,4-DIOXANE**

**ABSTRACT**

In this study, novel asymmetric membranes with pre-selective layer consist of electrospun poly(vinyl alcohol) (PVA) nanofibres and electrospun PVA nanofibres integrated with two different types of hydrophilic fillers i.e. micron-sized copper benzene-1,3,5-tricarboxylate (Cu-BTC) and nano-sized carboxyl multi-walled carbon nanotube (COOH-MWCNT), respectively were successfully fabricated. Electrospun PVA nanofibres, Cu-BTC/PVA and COOH-MWCNT/PVA composite nanofibres were deposited on dense PVA membranes to form  $M_0$ ,  $M_{CuBTC}$  and  $M_{COOH-MWCNT}$  asymmetric membranes, respectively. All asymmetric membranes showed improved performance in the pervaporation dehydration of aqueous 1,4-dioxane solutions. This phenomenon is due to the electrospun hydrophilic nanofibre layer serving as a hydrophilic pre-selective barrier that traps water molecules. The pervaporation separation performance increased in the following order: dense PVA membrane  $< M_0 < M_{COOH-MWCNT} < M_{CuBTC}$ . Compared to dense PVA membrane,  $M_0$  exhibited an increment of almost 50% in water permeation flux accompanied with an increase in separation factor. Between  $M_{CuBTC}$  and  $M_{COOH-MWCNT}$  membranes,  $M_{CuBTC}$  membranes exhibited better separation performance. The performance of the  $M_{CuBTC}$  membranes increases with increasing Cu-BTC loading of 0.5 to 1.0 wt.%. Among all the membranes studied,  $M_{CuBTC}$  membrane incorporated with 1.0 wt.% Cu-BTC ( $M_{CuBTC(1.0)}$ ) exhibited the highest permeation flux and separation factor with a total

permeation flux of  $87.69 \text{ g/m}^2 \cdot \text{h}$ , separation factor of up to 1852.32, water permeance of 2176.20 GPU, and water selectivity of 1417.52. The water permeation flux of the  $M_{\text{CuBTC}(1.0)}$  membrane was double of that of the dense PVA membrane, while the separation factor increased from 392.65 to 1852.32. When compared to  $M_0$ ,  $M_{\text{CuBTC}(1.0)}$  membrane provided an enhancement of nearly 40% in water permeation flux along with an increase in separation factor. However, among the  $M_{\text{COOH-MWCNT}}$  membranes integrated with 0.5 and 1.0 wt.% COOH-MWCNT, i.e.  $M_{\text{COOH-MWCNT}(0.5)}$  and  $M_{\text{COOH-MWCNT}(1.0)}$ , respectively, better separation performance was demonstrated by  $M_{\text{COOH-MWCNT}(0.5)}$  with a total permeation flux of  $75.71 \text{ g/m}^2 \cdot \text{h}$ , separation factor of 605.35, water permeance of 1836.08 GPU and membrane selectivity of 462.30 for water. An increment of around 80% and 20% in water permeation flux was achieved by the  $M_{\text{COOH-MWCNT}(0.5)}$  when compared to that of the dense PVA membrane and  $M_0$ , respectively. Although the separation factor of  $M_{\text{COOH-MWCNT}(0.5)}$  increased from 392.65 to 605.35 when compared to the dense PVA membrane, a slight decrease in separation factor from 682.11 to 605.35 was observed when compared to  $M_0$ . The parameters estimated using Rautenbach model showed that the dehydration of aqueous 1,4-dioxane solutions via pervaporation is dominantly governed by sorption process.

## **CHAPTER ONE**

### **INTRODUCTION**

An overview of the entire research project is presented in this chapter. The background and current development of pervaporation process is provided at the beginning of this chapter. In addition, electrospun nanofibres and their applications are briefly discussed. Then, the problem statement and objectives of this study are highlighted. Lastly, the scope of study and organization of the thesis are included at the end of this chapter.

#### **1.1 Pervaporation**

Pervaporation, a membrane-based separation technology, has attracted an exceptionally great amount of interest from researchers worldwide. It has been viewed as a potential alternative to the conventional separation techniques such as distillation process. In pervaporation, a dense membrane acts as a separating barrier and regulates the mass transport across the membrane. The feed liquid mixture is brought into contact with one side of the membrane where the component with higher affinity for the membrane will be preferentially transported across the membrane and removed from the other side of the membrane as a low pressure vapour. In order for separation to occur, the permeate side of the membrane is being held under vacuum or applying a sweep gas to create a chemical potential difference (Feng and Huang, 1997). The permeation of a component in membrane is driven by concentration and pressure gradients, and the overall driving force producing movement of a permeant is the chemical potential gradient. Schematic diagram of the pervaporation membrane cell operation is illustrated in Figure 1.1. The separation mechanism of the pervaporation

process primarily depends on the preferential sorption and diffusion of the target molecule through the membrane (Feng and Huang, 1997).

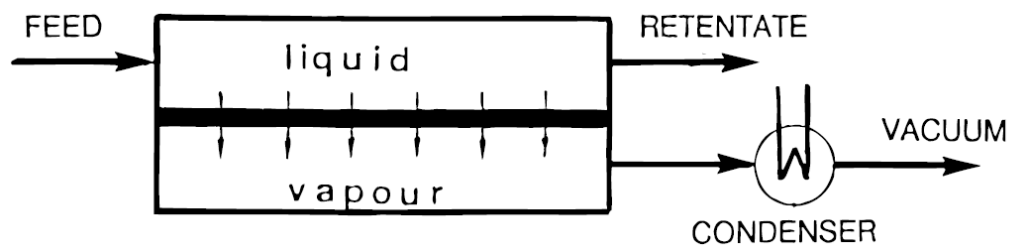


Figure 1.1: Schematic diagram of the pervaporation process (Feng and Huang, 1997).

In contrast to conventional distillation process which is an energy extensive process, pervaporation involves the removal of the minor components (usually less than 10 wt.%) of liquid mixtures which decreases the energy consumption since the heat energy needed for pervaporation process is merely the latent heat of evaporation for the minor component that permeates through the membrane (Shao and Huang, 2007). In addition, pervaporation process is able to separate close-boiling point and azeotropic mixture attributed to its separation principle based on the driving force induced by chemical potential gradient, affinity for the membrane and diffusivity of the components in the membrane (Vane, 2013) whereas azeotropic distillation process requires the addition of an entrainer. For the past few decades, pervaporation has been applied in dehydration of organic solvents, recovery of organic compounds from aqueous solutions and organic-organic mixtures separation. Up till now, pervaporation in dehydration of organic solvents is the most developed among these applications.

The term “pervaporation” was first defined by Kober in 1910s from the abbreviation of “permeation” and “evaporation” based on the selective permeation of water through the collodion and parchment membrane (Kober, 1917). In 1982, Gesellschaft für Trenntechnik, hamburg, Germany (now owned by Sulzer) installed

the first industrial scale pervaporation plant in Brazil for dehydration of ethanol/water azeotropic mixtures (Tusel and Brüscke, 1985). A composite membrane consists of a thin layer of crosslinked polyvinyl alcohol (PVA) coated on a porous poly(acrylonitrile) (PAN) support cast on a non-woven fabric was utilized (Tusel and Brüscke, 1985). The composite membrane was successful in breaking the azeotropic point of ethanol/water mixtures. Since then, pervaporation has undergone rapid development in large scale applications. At present, most of the pervaporation systems worldwide are dehydration of organic-aqueous mixtures. On the other hand, application of pervaporation in separation of organics from organic-aqueous mixtures and separation of organics from organic mixtures have been proven to be much more challenging due to the lack of appropriate membranes and modules that are able to endure continuous exposure of organic mixtures during the separation process (Baker, 2010).

## **1.2 Current development of membrane for pervaporation**

It is crucial for researchers to understand the fundamental of the mass transfer phenomena in order to be able to identify suitable membrane materials and design membranes with desired structure and configuration. In pervaporation, the mass transfer of the feed molecules is governed by the membrane which acts as a separating barrier and gatekeeper. Permeation of a feed molecule across the membrane is known as the rate-determining step (Nagai, 2010).

The solution-diffusion model, proposed by Thomas Graham to describe the gas transport through the diaphragms, is the most well-known and widely accepted transport mechanism for pervaporation (Huang, 1991, Wijmans and Baker, 1995, Feng and Huang, 1997, Baker, 2012). According to this mechanism shown in Figure 1.2,

the transport of a feed component across a membrane involves three consecutive steps:  
(i) Sorption of the permeating feed component into the upstream surface of the membrane; (ii) Diffusion of the permeating feed component across the membrane; (iii) Desorption of the permeating feed component to the vapour phase at the downstream of the membrane.

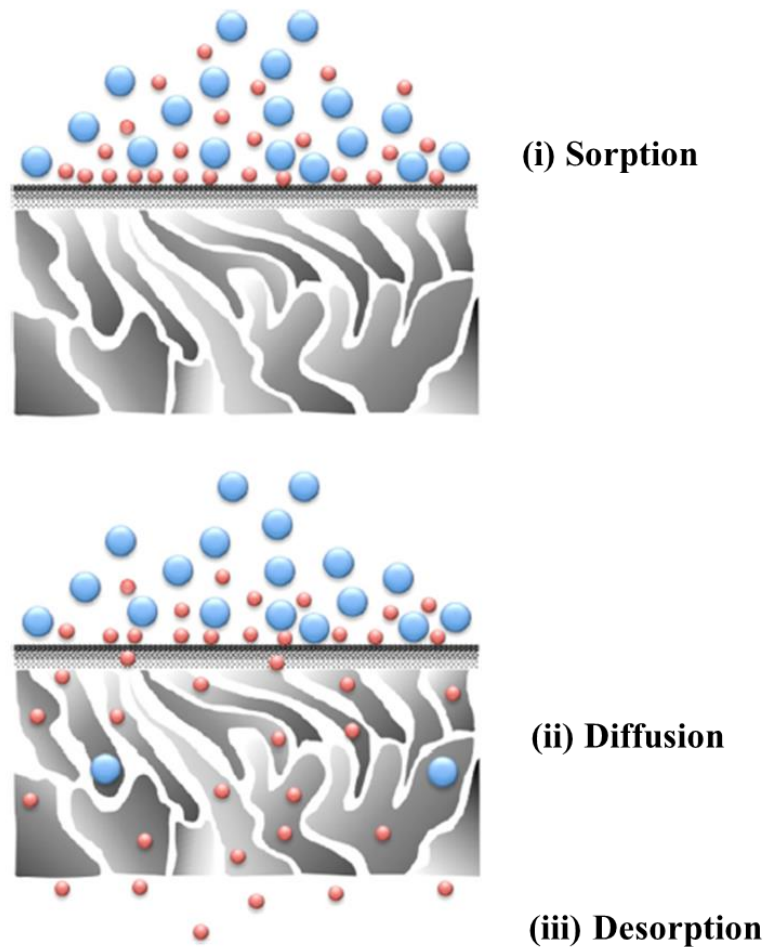


Figure 1.2 : Graphical representation of the solution-diffusion mechanism (Ong et al., 2016).

For that reason, enhanced separation performance can be achieved by improving the solubility selectivity and/or diffusivity selectivity of the penetrants across the membranes. The sorption selectivity of the membranes favours the

molecules which have the ability to establish special interactions with the membrane materials (Crespo and Bøddeker, 1994) whereas diffusion selectivity is very much affected by the size and shape of the permeating molecules, the flexibility of polymer chains and the interstitial space among them, the interactions between the permeating molecules and the membrane material as well as among the permeating molecules (Mulder, 1991). Therefore, the selection of the suitable membrane material is critical because the separation performance in pervaporation is heavily affected by the characteristics of the membrane used.

In general, the performance of a pervaporation membrane is assessed based on its productivity and capability to separate the desired components from the feed mixture. Permeation flux is commonly used to quantify the amount of component that permeate through a specific surface area of membrane over a given unit of time. The higher the permeation flux the more advantageous the membrane in pervaporation as the surface area of the membrane can be reduced. On the other hand, the ability of the membrane to eliminate a specific component from the feed mixture is represented by membrane selectivity which typically reflects the overall separation efficiency. Thus, a higher value of membrane selectivity guarantees higher separation efficiency. In addition, it is also important to take into account the physical and chemical stability of the membrane when selecting a suitable membrane to ensure that the separation performance is not compromised in harsh operating situations.

There are a variation of pervaporation membranes developed over the years. In general, the membranes can be classified as polymeric membrane, inorganic membrane and mixed matrix membrane (MMM) which comprises both organic and inorganic substances.

### 1.2.1 Polymeric membrane

Among all the different categories of membranes mentioned earlier, polymeric membranes are the most versatile and feasible because of their comparatively low production cost as well as ease of fabrication (Jiang et al., 2009). Polymeric membranes are considered dense membranes. Generally, there are two categories of polymeric membrane, namely glassy and rubbery polymeric membrane. While glassy polymer possesses a glass transition temperature above room temperature with rigid and strong properties due to the steric hindrance from polymer backbone that impedes the rotation of polymer segments, rubbery polymer is known to have a glass transition temperature below room temperature with soft and elastic properties attributed to the flexibility of polymer backbone which enable them to rotate freely around their axis (Ismail et al., 2009).

Some of the polymeric membranes which have demonstrated satisfactory separation performances in pervaporation process are PVA, chitosan (CS), polysulfone (PSF) and polydimethylsiloxane (PDMS). Nevertheless, polymeric membranes are known to suffer from short lifetimes, low thermal and chemical stabilities and low selectivity. The rubbery polymer, which exhibits excellent sorption behaviour, is often encountered with the issue of excessive swelling caused by the increase of the free volume between the polymer chains. Although this behaviour favours the permeation of components across the membrane, the selectivity of the membrane is eventually forfeited. Moreover, the excessive swelling of the membrane might lead to decreased mechanical stability in the end. As for the glassy polymer, its chain rigidity limits the mobility of the polymer chains which improves the mechanical strength of the membrane and reduces swelling. As a result, lower permeability of the membrane is inevitable in exchange for higher selectivity. Besides that, another major drawback in

the application of polymeric membranes is their limited solvent stability. Since polymeric membranes can be simply fabricated via solvent casting technique, excessive swelling or dissolution of the polymeric membranes may occur when they come into contact with a feed solution which contains its solvent, thereby destroying the separation barrier created by the membrane.

### **1.2.2 Inorganic membrane**

The shortcomings of polymeric membranes have led to the development of inorganic membranes with well-defined and regular pore structure such as zeolite and silica as an alternative candidate in membrane separation application due to their high physical, chemical and thermal stability (Peng et al., 2011). The exceptional properties of the inorganic membranes have caused them to be extensively investigated in membrane separation application, especially in harsh chemical situations.

The event of membrane failure caused by excessive swelling is not likely to happen in the case of inorganic membranes owing to their rigidity. Besides, inorganic membranes can be subjected to a wide range of solvent mixtures due to their outstanding solvent resistance property contributed by their chemical stability. Furthermore, inorganic membranes can be incorporated with metal oxides such as aluminium oxide, zirconia and titania to enhance their chemical stability (Sekulić et al., 2002). Promising results in separation performance displayed by inorganic membranes have been widely reported in dehydration of organic solvents and recovery of organic solvent from aqueous solutions (Zhou et al., 2012, Sawamura et al., 2015, Kujawa et al., 2015a, Kujawa et al., 2015b).

However, the realization of the application of inorganic membranes is still hindered by the membrane synthesis process, despite their encouraging prospects. In

addition to the concern regarding high synthesis cost, brittleness issue induced by the rigidity of the inorganic membranes which complicates membrane fabrication, particularly in the case of thin layer formation, remains a problem to be solved. Another shortfall is due to its relatively low separation ability or selectivity when compared to its polymeric counterparts.

### **1.2.3 Mixed matrix membranes (MMMs)**

The separation performances of both polymeric and inorganic membranes are restricted by the trade-off between permeability and selectivity. In other words, an increase in permeability is often accompanied by a decrease in selectivity and the other way round. Driven by the need to overcome this bottleneck situation, the development of MMM, which inherit advantageous properties from both the polymeric and inorganic membranes by combining polymer with inorganic materials, are growing rapidly in recent years.

The first MMM was developed by Barrer and James (1960a, 1960b). Since then, MMM has become a topic of interest in the development of membrane with improved separation performance. MMM is a relatively new class of membrane which is known to possess the flexibility of polymers and superior separation performance of inorganic fillers. Hence, it is strongly believed that the MMMs exhibit great potential in circumventing the trade-off phenomena and improving the robustness of the membrane in long-term operation owing to their outstanding features. The configuration of MMM is depicted in Figure 1.3, in which the inorganic fillers are dispersed homogeneously in the polymer phase. MMMs are endowed with numerous functionalities depending on the diverse combination of polymers and inorganic fillers.

The role of the inorganic fillers in the MMMs is to enhance the structural rigidity and decrease the free volume within the polymer matrix with the aim to improve membrane mechanical stability and prevent excessive swelling of the membrane. In addition, the incorporation of inorganic fillers in polymer matrix also contributes to enhanced thermal and chemical stabilities of the resultant MMMs. Meanwhile, the complication in processing of inorganic materials due to their brittleness is resolved by adopting polymer which is highly flexible as the continuous matrix.

Nevertheless, homogeneous distributions of inorganic fillers in polymer matrix should be emphasized to ensure good separation performance of the MMMs as the state of dispersion of the inorganic fillers crucially affects the separation performance of the MMMs. In reality, the inorganic fillers tend to form aggregation which may result in MMMs with undesirable defects such as the formation of voids between the inorganic fillers and polymer matrix, and compromised membrane mechanical properties. Thus, an ideal fabrication method should be able to confirm homogeneous dispersion of inorganic fillers in polymer matrix with the presence of sufficient interfacial bonding between the inorganic fillers and polymeric matrix.

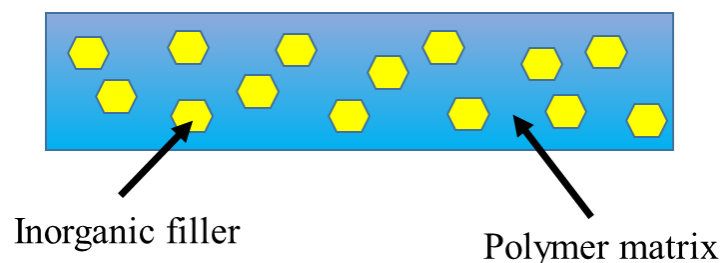


Figure 1.3 : Schematic diagram of a MMM.

### **1.3 Electrospun nanofibres and their applications**

When fibres sizes were reduced from micrometres to sub micrometres or nanometers, the surface area to volume ratio of the material could be increased tremendously. In this regard, very large surface area to volume ratio were obtainable, while having a greater mechanical strength and flexibility compared with larger fibres (Huang et al., 2003). Depending on the requirement, these nanofibres could be functionalized, integrated with fillers, or even used directly. Generally, nanofibres are classified as being less than 1 micrometre. Their excellent mechanical behaviour, high specific surface area, small pore size and a large pore volume, besides being lightweight in nature, make them attractive for many applications.

There are many ways to produce sub-micron or nanoscale fibre matrix. Some of the methods include template synthesis, fibre drawing, phase separation self-assembly and electrospinning. Among the techniques mentioned, electrospinning has been known as a simple and versatile technique to produce highly porous structures of ultrafine fibres with diameters ranging from nano- to micro-scale using various polymer materials. Unlike traditional membrane fabrication techniques such as phase inversion, electrospinning allows the formation of interconnected pores with uniform pore size and high porosity. Hence, based on their exceptional properties, electrospun nanofibre membranes have been exploited in many water purification applications such as filtration (Bazargan et al., 2011, Shukla and Cheryan, 2002, Sundarrajan et al., 2013, Park and Kim, 2017, Agyemang et al., 2016, Xu et al., 2017, Wasim et al., 2017), forward osmosis (Hoover et al., 2013, Huang et al., 2016, Pan et al., 2017, Tian et al., 2013) and membrane distillation (Shauly et al., 2017, Hou et al., 2017). Recently, the electrospinning technique has been employed in the fabrication of membranes for the pervaporation separation process. Hung et al. (2014) successfully fabricated

composite membranes comprising heterogeneous polyamide layers on electrospun substrates for ethanol dehydration.

#### **1.4 Problem statement**

1,4-Dioxane, a colourless synthetic heterocyclic organic compound commonly used as an organic solvent in the petrochemical and pharmaceutical industries, is highly miscible with water in all proportions and forms an azeotropic mixture at a water-to-dioxane ratio of 18:82 by mass. In addition, 1,4-dioxane forms close boiling point mixtures with water at various compositions, as the boiling point of 1,4-dioxane (101 °C) is close to that of water (Baker et al., 1991). Although distillation is an efficient separation process widely used in industry, azeotropic and close boiling point mixtures cannot be separated by distillation. Pervaporation has emerged as one of the most promising and economical separation techniques that can be used as an alternative to distillation.

In pervaporation, the membrane acts as separating barrier and a gatekeeper that selectively controls mass transfer. The feed component is selectively transported across the membrane based on the affinity of the component towards membrane. Thus, the selection of the membrane with suitable characteristics is a critical factor that impacts the separation performance in pervaporation process. In general, separation performance of pervaporation process is evaluated based on permeation flux and separation factor. Nevertheless, the issue of a trade-off between permeation flux and separation factor has been widely reported. In this case, membranes with high permeation flux are usually accompanied by low separation factor. Hence, driven by this constraint, there have been a growing number of researches in seeking or designing

better membrane materials and developing membrane with new configurations with the aim of further improving membrane separation performance.

As mentioned previously in section 1.3, electrospun nanofibres appeared to be a good candidate for many water purification applications because of their unique and interesting features including high surface area-to-volume ratios, high porosities, high flexibilities, good modifiabilities, and good water permeabilities (Nasreen et al., 2013). On top of that, electrospun nanofibres could be integrated with different fillers to bestow the nanofibres with different functionality depending on the objective and to enhance separation performance. As the objective of this study is to dehydrate 1,4-dioxane/water mixture, two different types of hydrophilic fillers with high surface area, namely micron-sized copper benzene-1,3,5-tricarboxylate (Cu-BTC) and nano-sized carboxyl multi-walled carbon nanotube (COOH-MWCNT) were integrated with the electrospun nanofibres. Cu-BTC is a relatively new porous solid material where its structure contains cages with hydrophilic open metal sites that preferentially adsorb polar molecules with high dipole moments such as water (Gutiérrez-Sevillano et al., 2013). On the other hand, the exceptionally smooth hollow structure of the CNT could facilitate rapid diffusive transport of liquid molecules via the inner channels. In addition, functionalization of CNT with hydrophilic COOH group (COOH-MWCNT) could facilitate the selective removal of the water molecules. On top of that, the reason for selecting micron-sized and nano-sized hydrophilic fillers in this study is to investigate the feasibility of integrating fillers of different size range within the electrospun nanofibres.

Combining the electrospinning technique with the advantages of hydrophilic fillers (Cu-BTC and COOH-MWCNT), this study focuses on the fabrication of novel asymmetric membranes with a pre-selective layer composed of electrospun PVA

composite nanofibres deposited on a thin layer of dense PVA. The schematic diagram of the proposed asymmetric membrane is shown in Figure 1.4. The configuration of the resulting membrane is different from that of a conventional asymmetric membrane, in which the electrospun hydrophilic nanofibre layer was expected to act as a pre-selective layer to selectively trap water molecules to improve the removal of water from the feed mixture. It has been reported by Yee et al. (2014) that the introduction of a buckypaper pre-selective layer on a dense membrane successfully enhanced the separation performance in pervaporation. To the best of my knowledge, studies involving the application of asymmetric membranes consist of electrospun nanofibres integrated with fillers for pervaporation dehydration of organic solvents are scarce. Thus, by harvesting the advantageous properties of both the electrospun nanofibres and the hydrophilic fillers via the introduction of a pre-selective layer, enhanced permeation flux and separation factor are expected in the pervaporation dehydration of 1,4-dioxane/water mixtures.

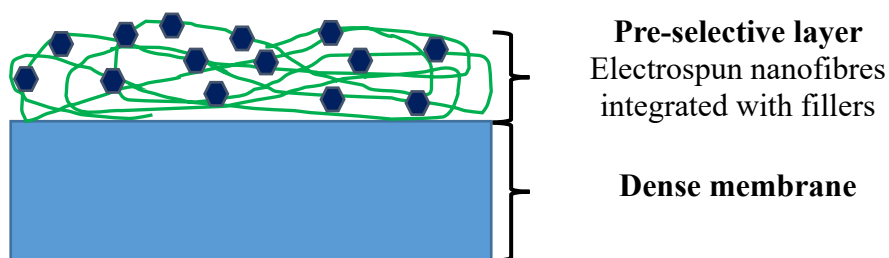


Figure 1.4: Schematic diagram of the proposed asymmetric membrane.

## 1.5 Objectives

The objective of this research is to investigate the pervaporation dehydration of 1,4-dioxane/water mixtures by the proposed asymmetric membranes.

- i. To develop and characterize  $M_{CuBTC}$  and  $M_{COOH-MWCNT}$  asymmetric membranes formed by electrospinning a suspension of Cu-BTC/PVA and COOH-MWCNT/PVA, respectively, onto preformed dense PVA membranes.
- ii. To study the effectiveness of the resultant asymmetric membranes in the pervaporation dehydration of 1,4-dioxane/water mixtures.
- iii. To investigate the effect of operating conditions (feed composition and feed temperature) on the separation performance of the asymmetric membranes in pervaporation.
- iv. To estimate the transport coefficient in pervaporation through the resultant asymmetric membranes via a semi-empirical flux model known as Rautenbach model.

## 1.6 Scope of the study

This research project is made up of three main sections; fabrication of novel asymmetric membranes, study of the effectiveness of the resultant asymmetric membranes in pervaporation dehydration process of 1,4-dioxane/water mixtures and the estimation of the transport coefficients of the pervaporation process using Rautenbach equation.

In this research project, three different asymmetric membranes as follows: asymmetric membrane with pre-selective layer of electrospun PVA nanofibres without fillers ( $M_0$ ),  $M_{CuBTC}$  and  $M_{COOH-MWCNT}$  were synthesized. In the fabrication of  $M_0$ , a

dense PVA membrane was prepared by solution casting technique, and then its surface was coated with a pre-selective layer made of PVA nanofibres via the electrospinning technique to produce an asymmetric membrane. The concentration of PVA solution for electrospinning were varied in order to determine the optimum concentration of PVA solution in order to obtain well-formed nanofibres. The morphologies of the as spun nanofibres were investigated via scanning electron microscope (SEM). Then,  $M_{CuBTC}$  and  $M_{COOH-MWCNT}$  asymmetric membranes were prepared with similar procedure where the pre-formed dense PVA membranes were coated with Cu-BTC/PVA and COOH-MWCNT/PVA composite nanofibres, respectively. The loading of Cu-BTC and COOH-MWCNTs were varied at 0.5 and 1.0 wt.%.

Next, the effectiveness of the dense PVA,  $M_0$ ,  $M_{CuBTC}$  and  $M_{COOH-MWCNT}$  membrane were investigated in the pervaporation dehydration of 1,4-dioxane/water mixtures. Prior to pervaporation process, the membranes were subjected to contact angle measurement and liquid sorption test in order to inspect the degree of hydrophilicity and the affinity of the membranes. After that, the membranes were applied in the pervaporation process in dehydrating 1,4-dioxane/water mixtures. The effect of electrospun nanofibres as the pre-selective layer was investigated followed by the study of the effects of operating parameters including feed concentration and feed temperature on pervaporation performance. The separation performances of the membranes were reported in terms of permeation flux, separation factor, permeance and selectivity.

Last but not least, the transport coefficients of the pervaporation process were estimated by Rautenbach equation in the final section.

## **1.7 Organization of the thesis**

There are five chapters in this thesis. Detailed information of the research project corresponding to each chapter's title is being presented in each chapter. A summary of the organization of this thesis is presented below.

Initially, a general overview of pervaporation process and the current development of the membranes used in pervaporation processes are provided in chapter one. A brief introduction on the electrospun nanofibres and their applications is provided. Next, it is followed by the problem statement emphasizing on the limitation of the recent membrane materials and highlighting the approach proposed in this research project. Subsequently, the objectives of this research project are stated followed by the scope of study and the overall organization of this thesis

Next, in chapter two, literature review on the topics related to this research project including the fabrication of electrospun nanofibres and its application in membrane separation process, background on Cu-BTC and CNTs and the application of metal organic frameworks (MOFs) and CNTs in pervaporation dehydration process. In addition, the recent developments in dehydration of 1,4-dioxane aqueous solution are also discussed followed by the fundamental on the estimation of transport coefficient using Rautenbach model.

Chapter three presents an overview of the experimental procedures involved in this research project. The fabrication and characterization methodologies of the proposed asymmetric membranes are described in detail. Apart from that, the operation of the pervaporation process and the mathematical equations that are required for the evaluation of the membrane performances are included. The application of semi-empirical model of Rautenbach to estimate the transport coefficients in pervaporation process is presented at the end of this chapter.

The findings of this research project are discussed in detail in chapter four. This chapter is divided into three sections. The first and second section includes the characterization and the capability of the asymmetric membranes in pervaporation dehydration of 1,4-dioxane/water mixtures for  $M_{CuBTC}$  and  $M_{COOH-MWCNT}$ , respectively. Meanwhile, the application of a semi-empirical mathematic model based on solution-diffusion theory known as Rautenbach model to estimate the transport coefficient of the pervaporation process using the asymmetric membranes are presented in the final section.

In chapter five, a conclusion based on the main discoveries of this research project is presented. Last but not least, recommendations for the future studies related to this research project are also proposed.

## **CHAPTER TWO**

### **LITERATURE REVIEW**

This chapter provides the literature review on the topics related to this research project. First, the working principle and the parameters affecting the electrospinning process were discussed. Subsequently, a review on the application of electrospun nanofibres in separation processes was included. An introduction of the MOF used in this study (Cu-BTC) was provided in the next section followed by the application of different types of MOF MMMs in various pervaporation processes. Then, the next section covers the introduction on CNTs and the application of CNT MMMs in different pervaporation applications. Later on, literature review on the different types of membranes used for the dehydration of 1,4-dioxane aqueous solution via pervaporation was provided. Lastly, the fundamental on the estimation of transport coefficient using Rautenbach model was discussed at the end of this chapter.

#### **2.1 Fabrication of electrospun nanofibres via electrospinning process**

Electrospinning refers to the process of producing fibres using electrostatic forces. Electrospinning process was first studied in detail by Zeleny (1914) and patented by Anton (1934). The foundation of electrospinning was developed by Taylor (1969) based on his work on electrically driven jets. In general, electrospinning is a simple experimental set-up comprising of a high voltage generator to draw fine strands of charged solutions across the air. Similar to conventional spinning process, the electrospinning process involves the act of drawing and subsequent conversion of liquid melt or solution into fibres. Unlike the traditional fibres production techniques such as mechanical extrusion or drawing, electrospinning utilizes an electrical

potential difference to create an electrostatic force to enable the drawing of liquid stream from the tip of the syringe to a collector (generally grounded or of opposing voltage). The liquid stream dries out as its solvent vaporizes on its journey towards the collector, resulting in the formation of thin, stretched fibres with diameters from nanometer to micrometer and a larger surface area than those produced via conventional spinning processes.

### **2.1.1 Working principle**

As illustrated in Figure 2.1, an electrospinning set up typically consists of three main components, which are the spinneret (e.g., a pipette or a syringe filled with polymer solution), a high voltage source and a grounded conductive collector. On top of that, the dispensing rate of the polymer solution can be controlled by the use of a syringe pump. Basically, the needle of the syringe acts as an electrode to electrically charge the polymer solution while the counter-electrode is connected to the conductive collector. The charged polymer solution is then accelerated towards the grounded conductive collector once the potential difference applied surpasses a limiting voltage necessary to overcome the surface tension of the liquid. In the process, the solvent vaporizes, the polymer jet undergoes continuous stretching and elongation until it reaches the collector forming a thin fibre (Adomavičiūtė and Milašius, 2007).

The potential difference is one of the critical elements in ensuring the feasibility of electrospinning. A threshold voltage, also known as critical voltage has to be achieved in order to initiate the process of electrospinning. Referring to Figure 2.2 (a), a pendant drop is formed at the tip of the pipette at low electrostatic field force owing to the surface tension of the solution (Reneker et al., 2000, Shin et al., 2001a,

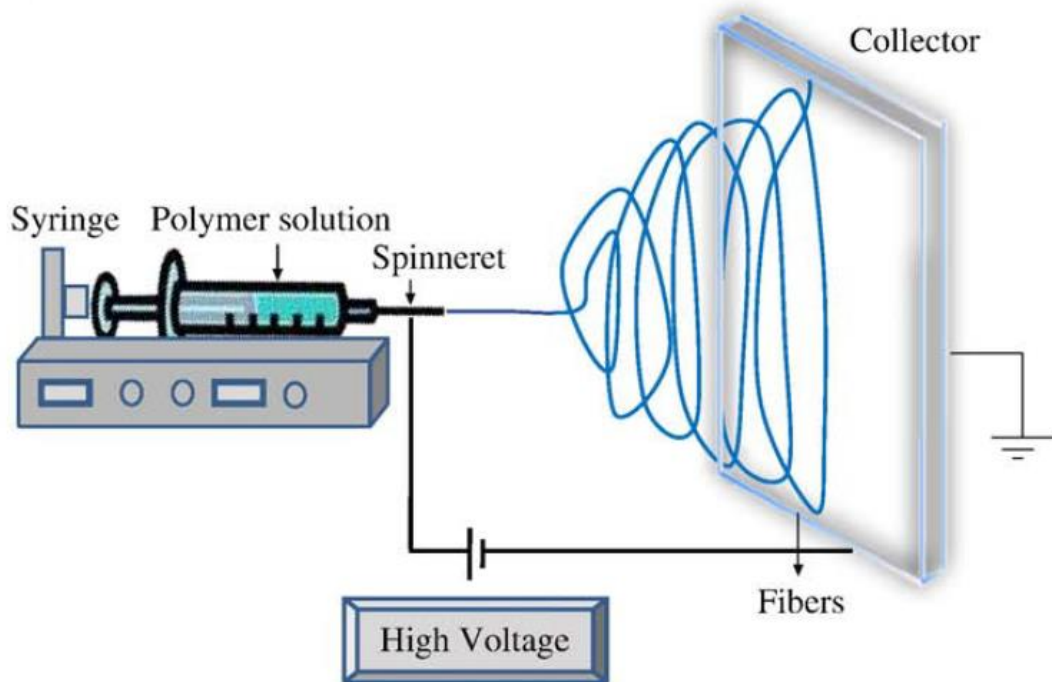


Figure 2.1: A basic electrospinning set up (Bhardwaj and Kundu, 2010).

Shin et al., 2001b). When the intensity of the electric field increases, the induced charges on the surface of the solution increases and start to repel each other. Thus, a repulsive force known as shear stress that act in a direction opposite to the surface tension is created (Fang and Reneker, 1997). Under these circumstances, the pendant drop extends into a conical shape, known as Taylor cone (Taylor, 1964, Taylor, 1969, Hohman et al., 2001a). Once the critical voltage is achieved, the electrical force is able to overcome the surface tension of the liquid and a charged jet emerges from the tip of the conical drop and accelerates towards the grounded collector. An illustration of the process is shown in Figure 2.2.

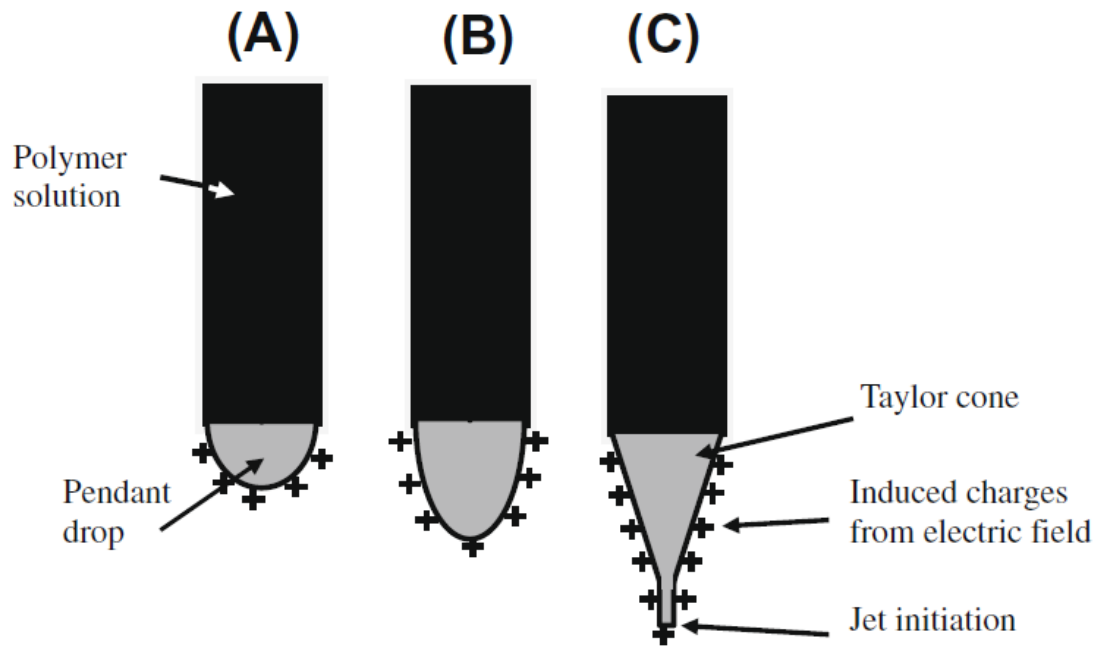


Figure 2.2: Schematic illustration of the Taylor cone formation: (A) Surface charges are induced in the polymer solution due to the electric field. (B) Elongation of the pendant drop. (C) Deformation of the pendant drop to the form the Taylor cone due to the charge-charge repulsion. A fine jet initiates from the cone (Baji et al., 2010).

### 2.1.2 Effects of various parameters on electrospinning

The various parameters affecting electrospinning process can be categorized into solution parameters and process parameters. Solution parameters consist of polymer concentration, viscosity, molecular weight, and surface tension while process parameters include applied voltage, tip to collector distance and flow rate of solution. The morphology of the electrospun fibres are significantly affected by these parameters. Hence, it is possible to obtain nanofibres of desired morphology and diameters with appropriate manipulation of these parameters (Chong et al., 2007).

### **2.1.2(a) Solution parameters**

#### **2.1.2(a)(i) Polymer concentration**

The formation of fibre in the electrospinning process requires a minimum solution concentration. Based on the findings of related studies (Deitzel et al., 2001, Liu and Hsieh, 2002, Ryu et al., 2003, McKee et al., 2004, Ki et al., 2005, Haghi and Akbari, 2007), a mixture of beads and fibres is formed at low solution concentration. It was also discovered that the shape of the beads changes from spherical to spindle-like and eventually uniform fibres with increased diameters were produced with increasing solution concentration because of the higher viscosity resistance. Hence, an optimum solution concentration should be determined for the electrospinning process. It has been found that the relationship between solution concentration and fibre diameter can be represented by a power law relationship where the fibre diameter increases with increasing solution concentration (Ki et al., 2005, Jun et al., 2003). In addition, the range of concentrations from which continuous fibres can be obtained in electrospinning are also dependent on the solution surface tension and viscosity (Deitzel et al., 2001).

#### **2.1.2(a)(ii) Molecular weight**

Molecular weight of the polymer also plays an important role in determining the morphology of the electrospun fibres. Variation in the molecular weight of the polymer significantly impacts the rheological and electrical properties including viscosity, surface tension, conductivity and dielectric strength (Haghi and Akbari, 2007). High molecular weight polymer solutions were usually used in electrospinning due to their higher viscosity which is desirable for fibre formation. With a solution of too low molecular weight, the tendency of beads formation is higher than fibres

whereas fibres with larger diameters were generated with a high molecular weight solution. Molecular weight of the polymer indicates the number of entanglements of polymer chains in a solution. Chain entanglement has a significant effect in the fibre formation in electrospinning. Tan et al. (2005) obtained a uniform jet during electrospinning of high molecular weight poly-L-lactic acid as sufficient number of entanglements of the polymer chains that guarantees an adequate level of solution viscosity were provided to restrain effects of surface tension, which contributes to the formation of beads on electrospun nanofibers. The effect of molecular weight of the polymer was studied using poly(methyl methacrylate) with molecular weight varying from 12.5 to 365.7 kDa (Gupta et al., 2005). It was found that the number of beads and droplets decreased with increasing molecular weight. On the other hand, via the electrospinning of oligomer-sized phospholipids generated from lecithin solutions, Mckee et al. (2006) and Burger et al. (2006) have discovered that as long as sufficient intermolecular interactions are able to provide a substitute for the inter-chain connectivity obtained from chain entanglements, the use of polymer with high molecular weights are not necessary for electrospinning process.

### **2.1.2(a)(iii) Viscosity**

In fact, viscosity, polymer concentration and molecular weight of polymer are all interrelated. Viscosity can be generally defined as the measure of the resistance of a fluid to flow. For fluid flow, a low viscosity fluid is desirable but this is not true for electrospinning. This is because a minimum viscosity is required to prevent the polymer jet from collapsing into droplets before it is dried to form fibres, a phenomena known as electrospraying (Frenot and Chronakis, 2003). Also, in the electrospinning of solution with low viscosities, beads or beaded fibres were obtained (Doshi and

Reneker, 1995). This is due to the fact that the probabilities of polymer entanglement is lower at lower viscosity, which is not sufficient to ensure jet stabilization, therefore uneven contraction in the fibres, and subsequent formation of beaded fibres were observed under the dominant influence of surface tension (Zhang et al., 2005).

On the other hand, an increase in solution viscosity or concentration results in larger and more uniform fibre diameter (Deitzel et al., 2001). Nonetheless, note has to be taken that the viscosity of the solution must not be too high that electrospinning is not feasible (Zhang et al., 2005). Judging from all these studies, a conclusion can be drawn that there should exist polymer-specific, optimal viscosity values for the formation of defect-free fibres via electrospinning. Figure 2.3 shows the variation in morphology of electrospun nanofibres with viscosity. As the viscosity increases, the shape of the beads evolved from droplet shape to elongated droplet followed by stretched droplet and finally forming uniform nanofibres.

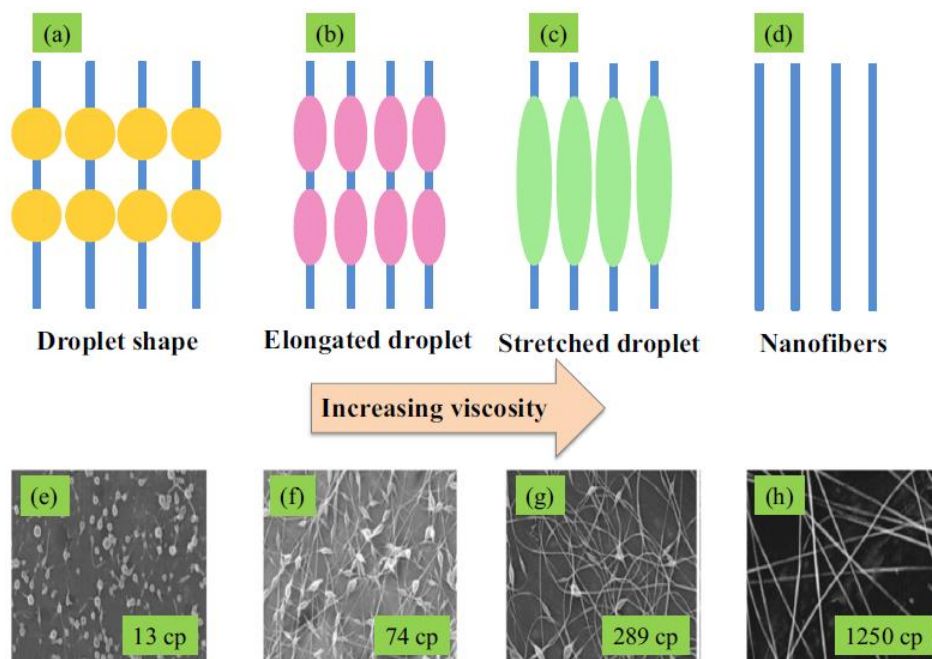


Figure 2.3: Variation in morphology of electrospun nanofibres of poly(ethylene oxide) with increasing viscosity: (a–d) schematic and (e–h) SEM micrographs (Haider et al., 2015).